

MT-PCR: A Hybrid Mamba-Transformer with Spatial Serialization for Hierarchical Point Cloud Registration

Bingxi Liu
SUSTech & PCL
Shenzhen, China
liubx@pcl.ac.cn

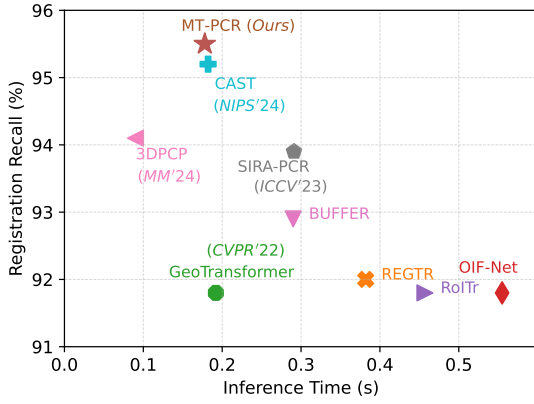
An Liu
Chongqing University
Chongqing, China
aliu@stu.cqu.edu.cn

Hao Chen
Cambridge University
Cambridge, United Kingdom
ch666@cam.ac.uk

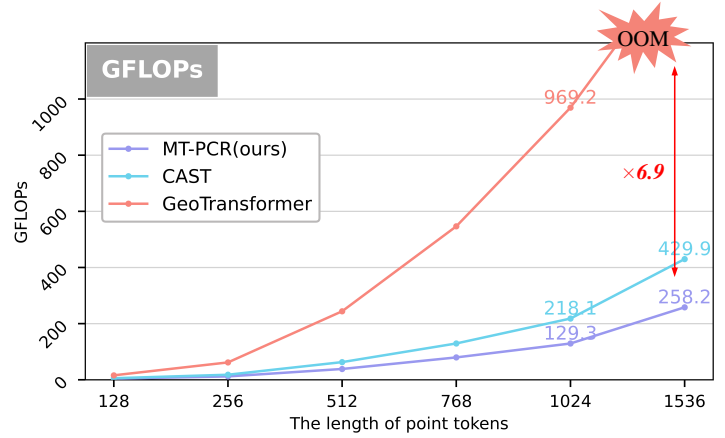
Jinqiang Cui
PCL
Shenzhen, China
cuijq@pcl.ac.cn

Yiqun Wang*
Chongqing University
Chongqing, China
yiqun.wang@cqu.edu.cn

Hong Zhang*
SUSTech
Shenzhen, China
hongz@sustech.edu.cn



(a) Registration Comparison



(b) FLOPs Comparison

Figure 1: Efficiency vs. Performance Trade-off of MT-PCR. (a) Registration recall vs. inference time comparison on 3DMatch. Our method, MT-PCR, achieves the best registration performance while maintaining competitive inference efficiency, outperforming recent state-of-the-art (SOTA) methods such as CAST (NIPS'24) and 3DPCP (MM'24). (b) FLOPs comparison under varying point token lengths. MT-PCR scales significantly better than GeoTransformer and CAST, maintaining low computational overhead even as the input size increases. Notably, GeoTransformer suffers from *out-of-memory* (OOM) issues at large resolutions, while MT-PCR remains efficient, achieving up to $6.9\times$ lower FLOPs at 1536 tokens.

Abstract

Point cloud registration (PCR) is a fundamental task in 3D computer vision and robotics. Most existing learning-based PCR methods rely on Transformers, which suffer from quadratic computational complexity. This limitation restricts the resolution of point clouds that can be processed, inevitably leading to information loss. In

*Corresponding author

Permission to make digital or hard copies of all or part of this work for personal or classroom use is granted without fee provided that copies are not made or distributed for profit or commercial advantage and that copies bear this notice and the full citation on the first page. Copyrights for components of this work owned by others than the author(s) must be honored. Abstracting with credit is permitted. To copy otherwise, or republish, to post on servers or to redistribute to lists, requires prior specific permission and/or a fee. Request permissions from permissions@acm.org.

MM '25, Dublin, Ireland

© 2025 Copyright held by the owner/author(s). Publication rights licensed to ACM.
ACM ISBN 978-1-4503-XXXX-X/18/06
<https://doi.org/XXXXXXX.XXXXXXX>

contrast, Mamba—a recently proposed model based on state space models (SSMs)—achieves linear computational complexity while maintaining strong long-range contextual modeling capabilities. However, directly applying Mamba to PCR tasks yields suboptimal performance due to the unordered and irregular nature of point cloud data. To address this challenge, we propose MT-PCR, the first point cloud registration framework that integrates both Mamba and Transformer modules. Specifically, we serialize point cloud features using Z-order space-filling curves to enforce spatial locality, enabling Mamba to better model the geometric structure of the input. Additionally, we remove the order indicator module commonly used in Mamba-based sequence modeling, leads to improved performance in our setting. The serialized features are then processed by an optimized Mamba encoder, followed by a Transformer refinement stage. Extensive experiments on multiple benchmarks

demonstrate that MT-PCR outperforms Transformer-based and concurrent state-of-the-art methods in both accuracy and efficiency, significantly reducing while GPU memory usage and FLOPs.

CCS Concepts

• **Theory of computation** → **Computational geometry**; • **Computing methodologies** → **Point-based models**.

Keywords

Point Cloud Registration, State Space Model, Attention Model

ACM Reference Format:

Bingxi Liu, An Liu, Hao Chen, Jinqiang Cui, Yiqun Wang, and Hong Zhang*. 2025. MT-PCR: A Hybrid Mamba-Transformer with Spatial Serialization for Hierarchical Point Cloud Registration. In *Proceedings of Proceedings of the 33rd ACM International Conference on Multimedia (MM '25)*. ACM, Dublin, Ireland, 10 pages. <https://doi.org/XXXXXXX.XXXXXXX>

1 Introduction

Point cloud registration (PCR) is a foundational task in 3D computer vision [40] and robotics [42], widely applied in tasks such as simultaneous localization and mapping (SLAM) [5], augmented reality (AR) [6], and autonomous driving [28]. PCR aims to estimate an optimal rigid transformation, aligning partially overlapping 3D point cloud pairs into a unified coordinate system. Despite significant advances, efficient and accurate PCR remains challenging due to complex spatial structures [39], partial overlaps [17], measurement noise, and large-scale scenes [27].

Recently, Transformer-based methods have shown remarkable performance improvements in PCR tasks by leveraging powerful self-attention and cross-attention mechanisms [32]. Transformers [37] can effectively model global spatial relationships and feature correspondences across point clouds, significantly outperforming hand-crafted or convolution-based approaches. However, Transformers inherently possess quadratic computational complexity with respect to sequence length [9], severely restricting their scalability and resolution capacity. Consequently, existing Transformer-based methods typically rely on downsampling point clouds to reduce computational overhead, inevitably losing important geometric information critical for precise alignment.

On the other hand, linear attention models, particularly the recently introduced Mamba model [15], have demonstrated promising results in efficiently capturing long-range contextual dependencies in sequential modeling tasks. Unlike Transformers, Mamba leverages linear complexity state-space architectures to approximate global context, thus significantly improving computational efficiency and scalability for long sequences. Nevertheless, directly applying the Mamba model to PCR tasks leads to suboptimal registration accuracy, primarily due to the loss of explicit spatial modeling and inadequate handling of unstructured point clouds.

Motivated by these observations, we propose MT-PCR, *the first* hierarchical point cloud registration framework that combines the efficient sequence modeling capabilities of Mamba with the bidirectional spatial awareness of cross-attention modules (Transformer). To effectively apply Mamba to irregular point cloud data, we introduce a feature serialization strategy based on Z-order space-filling

curves, which imposes spatial locality and improves the compatibility between point cloud structure and Mamba's sequence modeling paradigm. We further observe that removing the order-indicator tokens—typically used in Mamba for sequential tasks—results in improved registration performance on 3D data. Extensive experiments on standard PCR benchmarks, including the widely used 3DMatch [48], 3DLoMatch [20] and KITTI [13] datasets, demonstrate that MT-PCR significantly outperforms existing Transformer-based methods and concurrent SOTA approaches, as shown in Fig. 1. Moreover, our method achieves these improvements while drastically reducing GPU memory usage and computational overhead in terms of FLOPs, validating the scalability and efficiency of our hybrid architecture.

In summary, our contributions are three-fold:

- We introduce MT-PCR, the first hybrid Mamba-Transformer framework for hierarchical point cloud registration, leveraging linear-complexity sequence modeling and bidirectional cross-attention.
- We propose a spatially aware serialization method based on Z-order space-filling curves, enabling Mamba to effectively process unstructured 3D point cloud registration in a sequence format.
- We identify that the order indicator module, commonly adopted in Mamba-based sequence modeling, is unnecessary in our context, and its removal leads to improved performance in the PCR tasks.
- We conduct comprehensive experiments across multiple benchmarks, demonstrating that MT-PCR achieves state-of-the-art performance with significantly improved computational efficiency in both memory usage and FLOPs.

2 Related Work

2.1 Point Cloud Registration

PCR aims to estimate the rigid transformation between point clouds. Early methods primarily adopted hand-crafted descriptors to represent local features, typically leveraging local geometric attributes [36] or spatial distribution histograms [34] [35] for feature representation. However, their representational capacity is inherently constrained by hand-crafted feature, often leading to matching failures in noisy or complex scenarios.

Recently, learning-based 3D descriptors have demonstrated significant advantages. PerfectMatch [14] employs Smoothed Density Value representations to learn discriminative features. PPF [11] extracts globally context-aware patch-wise features using a PointNet [31]-based architecture. FCGF [10] innovatively utilizes a sparse 3D convolutional encoder-decoder network for dense descriptor learning. SpinNet [2] proposes a 3D cylindrical convolutional network with specialized coordinate system designs to achieve rotation invariance. Predator [20] integrates graph convolutions with cross-attention mechanisms, explicitly optimizing overlap region prediction for low-overlap scenarios.

Driven by Transformer architectures, studies have incorporated attention mechanisms into PCR networks to enhance robustness. CoFiNet [45] pioneers the integration of self-attention and cross-attention mechanisms for coarse-level feature matching, combined

with optimal transport theory to refine fine-grained correspondences. GeoTransformer [32] introduces geometry-enhanced self-attention and a local-to-global registration framework to ensure pose estimation consistency. RoITr [46] develops a rotation-invariant Transformer architecture based on point-pair features, strengthening the robustness of coarse-to-fine frameworks. DiffusionPCR [8] incorporates diffusion models to enable iterative feature matching refinement. CAST [19] integrates consistency-aware mechanisms and point-guided strategies to suppress interference from irrelevant regions while enhancing feature matching capabilities. These methods face inherent limitations due to the quadratic computational complexity $O(N^2)$ of Transformer architectures, imposing restrictions on processable point cloud resolution. Consequently, this results in inevitable loss of geometric details in high-density point clouds during downsampling processes.

2.2 State Space Models and Mamba

State Space Models (SSMs) [21] originate from control theory and have garnered attention as efficient alternatives to Transformers for sequence modeling. Classical SSMs such as S4 [16] demonstrate the ability to model long-range dependencies with linear complexity by leveraging diagonal-plus-low-rank state transitions and HiPPO initialization. These models often suffer from computational inefficiencies or limited scalability.

To address these issues, Mamba [15] introduces a selective SSM mechanism, where input-conditioned parameterization enables selective information flow. By combining input-dependent state updates with hardware-aware parallelization, Mamba achieves strong performance with linear inference time. Variants such as Vision Mamba [50] and Vmamba [25] adapt Mamba to image-level tasks through bidirectional and cross-selective scanning strategies, showcasing its potential as a backbone for visual understanding.

Recent works attempt to transfer the benefits of SSMs and Mamba to 3D point cloud data. MetaLA [9] integrates Mamba into a meta-sequential attention framework, emphasizing lightweight modeling for point cloud perception tasks. PointMamba [23, 24] employs an octree-based serialization scheme to impose order on the unordered point cloud data, thus enabling causal dependencies compatible with Mamba’s design. Mamba3D [18] extends this line of research by incorporating Mamba into a 3D-aware architecture. It enhances Mamba’s spatial awareness through local geometry integration and various pretraining strategies, demonstrating improved scalability and representational capacity on 3D datasets. Still, its design targets object-level recognition and does not explicitly address the unique demands of PCR. In contrast, our work proposes the first Mamba-based architecture specifically tailored for PCR. We also address the key challenges of unordered and non-causal modeling, and build a hierarchical framework that combines Mamba’s global modeling capabilities with local attention and cross-scale refinement.

3 Problem Definition

Given two partially overlapping 3D point clouds $X = \{\mathbf{x}_i \in \mathbb{R}^3 \mid i = 1, 2, \dots, M\}$ and $Y = \{\mathbf{y}_j \in \mathbb{R}^3 \mid j = 1, 2, \dots, N\}$, denoted as the source and target respectively, the goal of point cloud registration (PCR) is to estimate the optimal rigid transformation that aligns X to Y . This transformation is defined by a rotation matrix $\mathbf{R} \in \text{SO}(3)$

and a translation vector $\mathbf{t} \in \mathbb{R}^3$. The solution is typically obtained by minimizing the weighted sum of squared distances between corresponding point pairs in a predicted correspondence set C :

$$\min_{\mathbf{R}, \mathbf{t}} \sum_{(\mathbf{x}_k, \mathbf{y}_k) \in C} w_k \|\mathbf{R}\mathbf{x}_k + \mathbf{t} - \mathbf{y}_k\|_2^2, \quad (1)$$

where w_k denotes the weight for each correspondence $(\mathbf{x}_k, \mathbf{y}_k)$.

4 Method

In this section, we first introduce the background of Transformers and Mamba in Section 4.1. Then, we present an overview of our framework MT-PCR in Section 4.2. The spatial serialization strategy is described in detail in Section 4.3, followed by the design of the Mamba Encoder in Section 4.4. Finally, the loss functions used for training are discussed in Section 4.5.

4.1 Preliminaries

Attention Mechanisms and Transformer. Transformers, constructed by stacking self-attention and cross-attention modules, have been widely employed in PCR tasks to effectively model global dependencies and feature correspondences. The self-attention mechanism computes attention weights within the same point set to capture internal feature interactions, while cross-attention identifies correspondences between two distinct point sets. Formally, given queries \mathbf{Q} , keys \mathbf{K} , and values \mathbf{V} , attention is computed as follows:

$$\text{Attention}(\mathbf{Q}, \mathbf{K}, \mathbf{V}) = \text{softmax} \left(\frac{\mathbf{Q}\mathbf{K}^\top}{\sqrt{d_k}} \right) \mathbf{V}, \quad (2)$$

where d_k denotes the dimensionality of key vectors. Despite their effectiveness, Transformers suffer from quadratic computational complexity with respect to sequence length, limiting their scalability to larger point clouds.

State Space Models and Mamba. SSMs are considered as a linear time-invariant, multi-input multi-output (MIMO) systems. Mathematically, a continuous-time SSM is described by a set of ordinary differential equations (ODEs) as:

$$\mathbf{h}'(t) = \mathbf{A}\mathbf{h}(t) + \mathbf{B}\mathbf{x}(t), \quad (3)$$

$$\mathbf{y}(t) = \mathbf{C}\mathbf{h}(t) + \mathbf{D}\mathbf{x}(t), \quad (4)$$

where $\mathbf{x}(t) \in \mathbb{R}^L$, $\mathbf{h}(t) \in \mathbb{R}^N$, $\mathbf{y}(t) \in \mathbb{R}^L$, and $\mathbf{h}'(t) \in \mathbb{R}^N$ represent continuous-time input, hidden state, output, and the derivative of the hidden state, respectively. $\mathbf{A} \in \mathbb{R}^{N \times N}$ represents the state matrix, $\mathbf{B} \in \mathbb{R}^{N \times L}$ denotes the input matrix, $\mathbf{C} \in \mathbb{R}^{L \times N}$ corresponds the output matrix, and $\mathbf{D} \in \mathbb{R}^{L \times L}$ is the feed-through matrix.

The continuous-time can be discretized to a discrete-time SSM by zero-order hold (ZOH) discretization. The parameters \mathbf{A} and \mathbf{B} of the discrete-time SSM can be obtained by introducing the sampling step Δ and Taylor expansion. In this case, parameters can be approximated as:

$$\bar{\mathbf{A}} = \exp(\Delta\mathbf{A}), \quad \bar{\mathbf{B}} = (\exp(\Delta\mathbf{A}) - \mathbf{I}) (\Delta\mathbf{A})^{-1} \cdot \Delta\mathbf{B}, \quad (5)$$

which results in the discrete form:

$$\mathbf{h}_k = \bar{\mathbf{A}}\mathbf{h}_{k-1} + \bar{\mathbf{B}}\mathbf{x}_k, \quad (6)$$

$$\mathbf{y}_k = \bar{\mathbf{C}}\mathbf{h}_k + \bar{\mathbf{D}}\mathbf{x}_k, \quad (7)$$

where \mathbf{x}_k , \mathbf{h}_k , and \mathbf{y}_k represent discrete-time input, state, and output vectors, respectively.

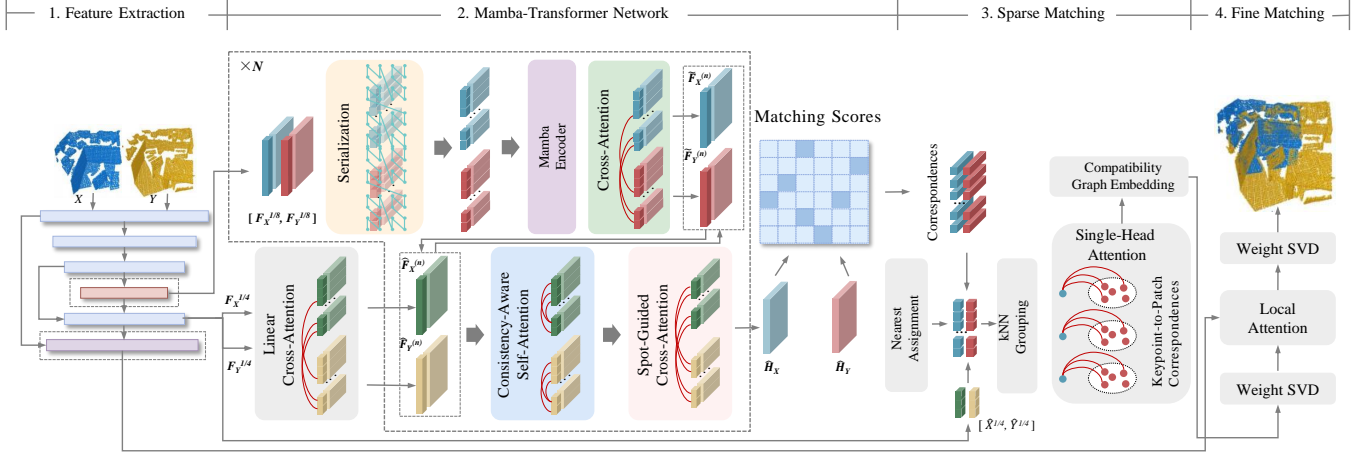


Figure 2: Overview of the MT-PCR Framework. The proposed pipeline consists of four stages: multi-scale feature extraction, coarse matching, sparse correspondence refinement, and fine registration. Notably, the coarse matching stage incorporates Mamba encoders with spatial serialization to model global geometric context efficiently.

Inspired by the above formulations, Gu and Dao proposed the Mamba model [15]—a novel variant of the SSM introducing input-dependent and time-varying system parameters. Specifically, parameters Δ , A , and B dynamically adapt according to the input x_t . The Mamba model achieves sequence-modeling performance comparable to Transformers, but crucially maintains linear computational complexity during inference. Although direct parallel computation is challenging, this issue addressed via a global convolutional expansion:

$$\mathbf{K} = (\overline{\mathbf{C}\mathbf{B}}, \overline{\mathbf{C}\mathbf{A}\mathbf{B}}, \dots, \overline{\mathbf{C}\mathbf{A}^{M-1}\mathbf{B}}), \quad \mathbf{y} = \mathbf{x} * \mathbf{K}, \quad (8)$$

where M denotes the input sequence length and \mathbf{K} represents the global convolution kernel. This convolutional formulation significantly improves computational efficiency. Further details can be referred to in the Mamba framework [15].

4.2 MT-PCR Overview

As illustrated in Fig. 2, MT-PCR employs a coarse-to-fine, multi-level feature matching architecture to achieve accurate PCR. It consists of the following key steps:

Multi-scale Feature Extraction: The Kernel Point Convolution (KPConv) is utilized to encode input point clouds into multi-scale feature representations spanning from the original dense point cloud (level L_0) to coarser downsampled point clouds (level L_k). The decoder-generated feature maps is denoted $\mathbf{F}^{1/k} = \{\mathbf{F}_X^{1/k}, \mathbf{F}_Y^{1/k}\}$, corresponding to nodes $X^{1/k}$ and $Y^{1/k}$, downsampled from the original point clouds X and Y , respectively. The key points at the topmost downsampling level are termed superpoints, serving as anchor points for subsequent feature matching.

Mamba-Transformer Coarse Matching: Stacked Mamba feature extraction modules are applied at the superpoint level to construct correspondence sets $C_s = \{(x_i, y_j)\}$ within overlapping local regions. Based on these correspondences, a differentiable matching

matrix $\mathbf{M} \in \mathbb{R}^{N_s \times N_s}$ is constructed via compatibility graph convolutional networks, where each matrix element m_{ij} indicates the matching confidence between superpoint pairs (x_i, y_j) .

Sparse correspondence refinement: Based on coarse matching results, discriminative keypoints are identified within semi-dense node neighborhoods denoted as $X^{1/4}$ and $Y^{1/4}$. Virtual correspondences for these keypoints are then predicted using a lightweight attention module. To further eliminate spatially inconsistent outliers, a compatibility graph embedding network is employed, yielding a set of high-confidence inliers I_{inlier} .

Fine Registration. An alignment between the source $X^{1/2}$ and the target $Y^{1/2}$ is performed first using the initial transformation $(\hat{\mathbf{R}}_0, \hat{\mathbf{t}}_0)$. Then, a lightweight local attention module is applied to the point sets to estimate refined dense correspondences. These correspondences are then used to compute the final rigid transformation $(\hat{\mathbf{R}}, \hat{\mathbf{t}})$ via weighted SVD.

Challenges and Insights. Replacing the self-attention module with the Mamba module offers a promising pathway toward efficient global modeling due to its linear-time complexity. However, this substitution poses a fundamental challenge: **point clouds are inherently unordered and spatially irregular**, while Mamba is designed for causal, structured sequences as found in natural language processing. Unlike Transformers, which are permutation-invariant and better suited for unordered inputs, Mamba requires well-structured sequential inputs to operate effectively. This discrepancy raises a critical question: *How can we convert 3D point cloud data into meaningful one-dimensional sequences suitable for Mamba while preserving spatial coherence and geometric information?*

To overcome these challenges, we introduce a traversal serialization strategy along with its variants to generate multiple sequences of point clouds. This approach maximizes the retention of topological associations through multi-path spatial traversal. Additionally, we further observe that removing the order-indicator

tokens—typically used in Mamba for sequential tasks—results in improved registration performance.

4.3 Z-order-based Spatial Serialization

Algorithm 1: Z-order Encoding for 3D Point Clouds

Input: Grid coordinates $G = \{(x_i, y_i, z_i)\}_{i=1}^N$; depth d ; batch labels \mathbf{b}
Output: Z-order serialization code $\pi(\mathbf{p}_i)$ for each point
foreach $\mathbf{p}_i = (x_i, y_i, z_i) \in G$ **do**
 Convert x_i, y_i, z_i to d -bit binary integers;
 Interleave bits from (x_i, y_i, z_i) to get Morton code m_i ;
 if batch labels \mathbf{b} are provided **then**
 Concatenate batch ID as prefix:
 $m_i \leftarrow (\text{batch}_i \ll 3d) \mid m_i$
 end
end
return Z-order code list $\{\pi(\mathbf{p}_i) = m_i\}_{i=1}^N$

The superpoint features $\mathbf{F}^{1/k}$ obtained from KPConv are inherently unordered, which poses challenges for state space models like Mamba that rely on directional, sequential processing. To enable effective sequence modeling, we convert the 3D point cloud into a one-dimensional sequence while preserving spatial locality.

Formally, given a point cloud $\mathcal{X} = \{\mathbf{x}_i \mid \mathbf{x}_i \in \mathbb{R}^3, i = 1, \dots, N\}$, we define a bijective serialization function $f: \mathbb{R}^3 \rightarrow \mathbb{R}$ that maps each point to a scalar index: $f: \mathbf{x}_i \mapsto s_i, s_i \in \mathbb{R}, \forall \mathbf{x}_i \in \mathcal{X}$.

Among various strategies, space-filling curves (SFCs) like the Z-order curve (Morton code) are particularly effective, as they preserve spatial locality:

$$\|\mathbf{x}_i - \mathbf{x}_j\|_2 \approx 0 \Rightarrow |s_i - s_j| \approx 0. \quad (9)$$

This ensures that neighboring points in 3D space remain adjacent in the serialized 1D sequence, which is critical for maintaining structural coherence in Mamba-based modeling.

As show in Algorithm 1, we adopt Z-order serialization by first quantizing 3D coordinates to a discrete grid, then interleaving the bits of the d -bit integer representations of (x, y, z) to compute Morton codes. The resulting Z-order indices $\pi(\mathbf{p}_i)$ define a spatially-aware serialization path, enabling Mamba to effectively process the point cloud sequence while preserving geometric proximity.

4.4 Mamba Encoder

After serialization, the feature tokens \mathbf{z} are passed through an encoder composed of N stacked Mamba blocks to extract hierarchical geometric features. Each block consists of Layer Normalization (LN), a Selective State Space Model (SelectiveSSM), depth-wise separable convolutions (DW), and residual connections. The architecture is illustrated in Fig. 3, and the forward propagation for the l -th block can be described as:

$$F'_{l-1} = \text{LN}(F_{l-1}), \quad (10)$$

$$F'_l = \sigma \left(\text{DW} \left(\text{Linear} \left(F'_{l-1} \right) \right) \right), \quad (11)$$

$$F''_l = \sigma \left(\text{Linear} \left(F'_{l-1} \right) \right), \quad (12)$$

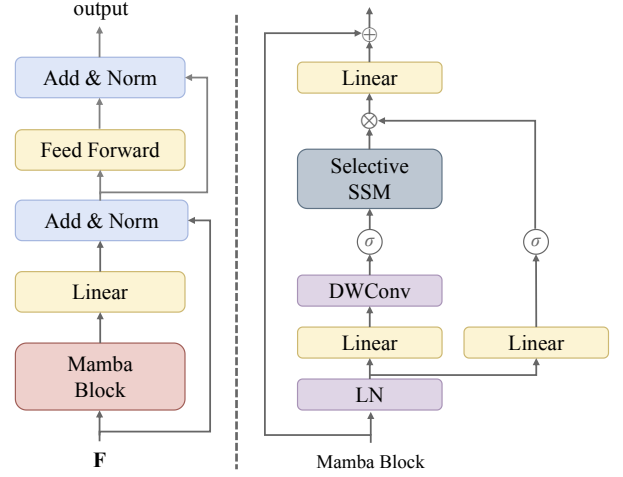


Figure 3: Architecture of the Mamba Encoder and Block. The left diagram illustrates the Mamba Encoder with residual connections and feed-forward networks (FNNs). The right diagram shows the internal structure of a Mamba Block, which centers around the SelectiveSSM.

$$F_l = \text{Linear} \left(\text{SelectiveSSM}(F'_l) \odot F''_l \right) + F_{l-1}, \quad (13)$$

where $F_l \in \mathbb{R}^{2n \times C}$ denotes the output features, and σ represents the SiLU activation function. The SelectiveSSM forms the core of the Mamba block, adaptively modeling contextual dependencies through input-conditioned parameterization. We adopted a minimalist yet effective design that complies with Occam’s razor [23], simplifying the implementation while retaining its expressiveness.

4.5 Loss Functions

Our overall loss function supervises four key modules in the hierarchical registration framework: *keypoint detection*, *coarse matching*, *keypoint matching*, and *dense registration*. Each sub-objective is addressed with a tailored loss component to guide the network effectively at different stages of alignment.

Keypoint Detection. To supervise the keypoint detec [22], denoted as \mathcal{L}_p . This loss encourages spatial alignment between predicted keypoints from the source and target point clouds while accounting for uncertainty. Specifically, we define:

$$\mathcal{L}_p = \frac{1}{N} \sum_{i=1}^N \left(\log \tilde{\sigma}_i + \frac{\|\mathbf{x}_i - \mathbf{y}_{j^*(i)}\|}{\tilde{\sigma}_i} \right) + \frac{1}{M} \sum_{j=1}^M \left(\log \tilde{\sigma}_j + \frac{\|\mathbf{y}_j - \mathbf{x}_{i^*(j)}\|}{\tilde{\sigma}_j} \right), \quad (14)$$

where $\mathbf{x}_i \in \mathbb{R}^3$ and $\mathbf{y}_j \in \mathbb{R}^3$ are keypoints from the reference and transformed point clouds, respectively. The indices $j^*(i) = \arg \min_j \|\mathbf{x}_i - \mathbf{y}_j\|$ and $i^*(j) = \arg \min_i \|\mathbf{y}_j - \mathbf{x}_i\|$ denote nearest neighbors. The uncertainty-aware weighting term $\tilde{\sigma}$ is computed

as the average predicted variance from both matched keypoints:

$$\tilde{\sigma}_i = \frac{1}{2} \left(\sigma_{x,i} + \sigma_{y,j^*(i)} \right), \quad \tilde{\sigma}_j = \frac{1}{2} \left(\sigma_{y,j} + \sigma_{x,i^*(j)} \right). \quad (15)$$

Coarse Matching. We utilize two weighted cross-entropy losses: the spot matching loss \mathcal{L}_s for layer-wise coarse scores $\mathbf{P}^{(l)}$ and the coarse matching loss \mathcal{L}_c for final coarse scores \mathbf{P} :

$$\begin{aligned} \mathcal{L}_s &= -\frac{1}{L} \sum_{l=1}^L \frac{1}{\sum_{(i,j) \in C} o_{ij}} \sum_{(i,j) \in C} o_{ij} \log \mathbf{P}_{ij}^{(l)}, \quad (16) \\ \mathcal{L}_c &= -\frac{1}{\sum_{(i,j) \in C} o_{ij}} \sum_{(i,j) \in C} o_{ij} \log \mathbf{P}_{ij} - \frac{1}{|\mathcal{N}_X|} \sum_{k \in \mathcal{N}_X} \log(1 - \hat{\sigma}_k^X) \\ &\quad - \frac{1}{|\mathcal{N}_Y|} \sum_{k \in \mathcal{N}_Y} \log(1 - \hat{\sigma}_k^Y), \quad (17) \end{aligned}$$

where \mathcal{N}_X and \mathcal{N}_Y denote sets of semi-dense nodes in the source and target point clouds without correspondences. The overlap ratio o_{ij} measures how much two local patches overlap. Further details can be referred to in the CAST [19].

Keypoint Matching. We employ three losses to supervise the similarity estimation, correspondence prediction, and consistency filtering. First, we use InfoNCE loss [29] \mathcal{L}_f to maximizing the similarity between descriptors d_x and d_{p_x} of true correspondences (x, p_x) and minimizing the similarity between descriptors d_x and d_{n_x} of false correspondences (x, n_x) :

$$\mathcal{L}_f = -\mathbb{E}_{(x, p_x, N_x)} \left[\log \frac{e(d_x^T W d_{p_x})}{e(d_x^T W d_{p_x}) + \sum_{n_x \in N_x} e(d_x^T W d_{n_x})} \right]. \quad (18)$$

where W is a symmetric learnable weight matrix. Next, an L_2 loss \mathcal{L}_k supervises predicted correspondences \hat{y} by minimizing:

$$\mathcal{L}_k = \mathbb{E}(x, \hat{y}) \|\mathbf{R}\mathbf{x} + \mathbf{t} - \hat{y}\|_2. \quad (19)$$

Finally, for consistency filtering, we define binary ground-truth labels based on whether the correspondence is an inlier (distance under threshold R_f), and supervise inlier confidence using binary cross-entropy:

$$\mathcal{L}_i = \text{BCE}(\text{score}, \text{inlier label}). \quad (20)$$

Dense Registration. The dense registration module is supervised using translation and rotation losses:

$$\mathcal{L}_t = \|\hat{\mathbf{t}} - \mathbf{t}\|_2, \quad \mathcal{L}_R = \|\hat{\mathbf{R}}^T \mathbf{R} - \mathbf{I}\|_F. \quad (21)$$

The final training loss is formulated as:

$$\mathcal{L} = \mathcal{L}_p + \lambda_s \mathcal{L}_s + \lambda_c \mathcal{L}_c + \lambda_f \mathcal{L}_f + \lambda_k \mathcal{L}_k + \lambda_i \mathcal{L}_i + \lambda_t \mathcal{L}_t + \lambda_R \mathcal{L}_R, \quad (22)$$

where $\lambda_s, \lambda_c, \lambda_f, \lambda_k, \lambda_i, \lambda_t, \lambda_R$ are hyper-parameters used to balance the contribution of each term by aligning their numerical scales.

5 Evaluation

In this section, we conduct extensive experiments to evaluate the performance of our proposed MT-PCR on both indoor RGB-D point cloud datasets (3DMatch [48] and 3DLoMatch [20]) and the outdoor LiDAR dataset (KITTI [13]).

5.1 Implementation Details

We employ the AdamW [26] optimizer with a batch size of 1, an initial learning rate of 1×10^{-4} , and a weight decay of 1×10^{-4} . A step-wise learning rate scheduler is adopted, decaying the learning rate by 10% every 5 training steps. Gradient clipping with a threshold of 0.5 is used to stabilize the training process. All experiments are conducted on a single NVIDIA RTX 3090 GPU. The number of training epochs is set to 5 for 3DMatch and 40 for KITTI.

5.2 Indoor Scenes: 3DMatch & 3DLoMatch

As shown in Table 1, we evaluate our method on the widely used indoor PCR benchmarks 3DMatch [48] and 3DLoMatch [20], which cover high-overlap ($>30\%$) and low-overlap ($10\%-30\%$) scenarios, respectively. We adopt a multi-dimensional evaluation framework. The primary metric is Registration Recall (RR), and efficiency is assessed via FLOPs and memory usage to provide a holistic view of computational performance.

All methods are re-implemented in a unified PyTorch [30] environment and tested under identical hardware settings (RTX 3090 GPU) to ensure fair comparisons of runtime and resource usage. We benchmark against state-of-the-art descriptor-based feature matching approaches and non-iterative correspondence-based registration methods. To enhance robustness, we apply RANSAC [12] post-processing for transformation estimation.

On the 3DMatch dataset, our method achieves a new state-of-the-art RR of 95.5%. On the more challenging 3DLoMatch dataset, MT-PCR reaches 75.4% RR, surpassing all descriptor-based baselines and non-iterative matching techniques. Notably, thanks to the linear attention mechanism introduced via Mamba, our approach demonstrates superior efficiency, achieving the fastest runtime among all compared methods.

Although our performance on 3DLoMatch slightly lags behind PEAL and DiffusionPCR in terms of RR, both methods incur over $10\times$ runtime overhead compared to ours. This efficiency-accuracy trade-off is especially valuable for real-world applications with limited computational budgets.

5.3 Outdoor Scenes: KITTI Odometry

As shown in Table 2, we further evaluate our method on the widely-used KITTI Odometry [13] dataset, which is a standard benchmark for autonomous driving scenarios. Following common practice, we adopt the standard split: sequences 00–05 are used for training, sequences 06–07 for validation, and sequences 08–10 for testing. To ensure high-quality training samples, we select point cloud pairs with a minimum spatial distance of 10 meters. The ground-truth transformations are obtained by aligning GPS/IMU trajectories refined by ICP.

The performance of MT-PCR is assessed using three commonly used metrics: Relative Rotation Error (RRE), Relative Translation Error (RTE), and Registration Recall (RR). We compare MT-PCR against a comprehensive set of state-of-the-art methods, including descriptor-based methods such as FCGF [10], D3Feat [4], SpinNet [2], and Predator [20], as well as correspondence-based approaches including CoFiNet [45], GeoTransformer [32], OIF-Net [41], PEAL [47], DiffusionPCR [8], MAC [49], and CAST [19].

Table 1: Evaluation results on indoor RGBD point cloud datasets.

Dataset		3DMatch					3DLoMatch					Average
Samples		Registration Recall (%)					Registration Recall (%)					Time (s) All
Descriptor-based	PerfectMatch [14]	78.4	76.2	71.4	67.6	50.8	33.0	29.0	23.3	17.0	11.0	-
	FCGF [10]	85.1	84.7	83.3	81.6	71.4	40.1	41.7	38.2	35.4	26.8	0.271
	D3Feat [4]	81.6	84.5	83.4	82.4	77.9	37.2	42.7	46.9	43.8	39.1	0.289
	SpinNet [2]	88.6	86.6	85.5	83.5	70.2	59.8	54.9	48.3	39.8	26.8	90.804
	YOHO [38]	90.8	90.3	89.1	88.6	84.5	65.2	65.5	63.2	56.5	48.0	13.529
	Predator [20]	89.0	89.9	90.6	88.5	86.6	59.8	61.2	62.4	60.8	58.1	0.759
Correspondence-based	REGTR [44]			92.0					64.8			0.382
	GeoTransformer [32]	92.0	91.8	91.8	91.4	91.2	75.0	74.8	74.2	74.1	73.5	0.192
	OIF-Net [41]	92.4	91.9	91.8	92.1	91.2	76.1	75.4	75.1	74.4	73.6	0.555
	RoITr [46]	91.9	91.7	91.8	91.4	91.0	74.7	74.8	74.8	74.2	73.6	0.457
	PEAL [47]	94.4	94.1	94.1	93.9	93.4	79.2	79.0	78.8	78.5	77.9	2.074
	BUFFER [1]			92.9					71.8			0.290
	SIRA-PCR [7]	93.6	93.9	93.9	92.7	92.4	73.5	73.9	73.0	73.4	71.1	0.291
	DiffusionPCR [8]	94.4	94.3	94.5	94.0	93.9	80.0	80.4	79.2	78.8	78.8	1.964
	CAST [19]			95.2					75.1			0.182
	MT-PCR (<i>ours</i>)			95.5					75.4			0.178

Table 2: Registration performance on KITTI dataset.

Model	RTE (cm)	RRE (°)	RR (%)
3DFeat-Net [43]	25.9	0.25	96.0
FCGF [10]	9.5	0.30	96.6
D3Feat [4]	7.2	0.30	99.8
SpinNet [2]	9.9	0.47	99.1
Predator [20]	6.8	0.27	99.8
CoFiNet [45]	8.2	0.41	99.8
GeoTrans [32]	6.8	0.24	99.8
OIF-Net [41]	6.5	0.23	99.8
PEAL [47]	6.8	0.23	99.8
DiffusionPCR [8]	6.3	0.23	99.8
MAC [49]	8.5	0.40	99.5
CAST [19]	2.5	0.27	100.0
MT-PCR (<i>ours</i>)	2.6	0.16	100.0

Experimental results demonstrate that our method achieves state-of-the-art performance in both RR and RRE, surpassing the current best model (DiffusionPCR) by a significant margin of 30.4% in rotation estimation. This indicates MT-PCR’s strong capability in predicting accurate rotations. Although the RTE reported by our method shows slight differences compared to the current SOTA

approaches, it still demonstrates comparable accuracy and strong consistency, fully validating its robustness and overall performance in outdoor LiDAR data processing.

5.4 Qualitative Results

Fig. 4 provide qualitative results about the registration performance on 3DMatch. Compared to CAST, our MT-PCR produces more accurate alignment results, especially in challenging regions highlighted by red boxes. The registered scenes by MT-PCR are visibly closer to the ground-truth, demonstrating its superior robustness and geometric consistency.

5.5 Ablation Study

Structural Efficiency. A core motivation of our work is to address the quadratic time complexity $O(N^2)$ and high resource consumption inherent in Transformer-based PCRs. To evaluate the efficiency of our design, we conduct a scalability study by varying the serialized point cloud sequence length and measuring performance in terms of FLOPs and memory usage.

We adopt a progressive stress-testing strategy on a 24GB VRAM GPU, gradually increasing input sequence length until memory constraints are reached. As shown in Table 3, our method achieves superior inference speed and lower GFLOPs across all lengths. Specifically, at a sequence length of 1536, our method reduces computation cost by 85.4% (to 1/6.9 GFLOPs) and memory usage by 58.3% (to 1/2.4) compared to a Transformer baseline—while maintaining comparable or better performance. This highlights the significant computational advantage of our model for long sequence modeling.

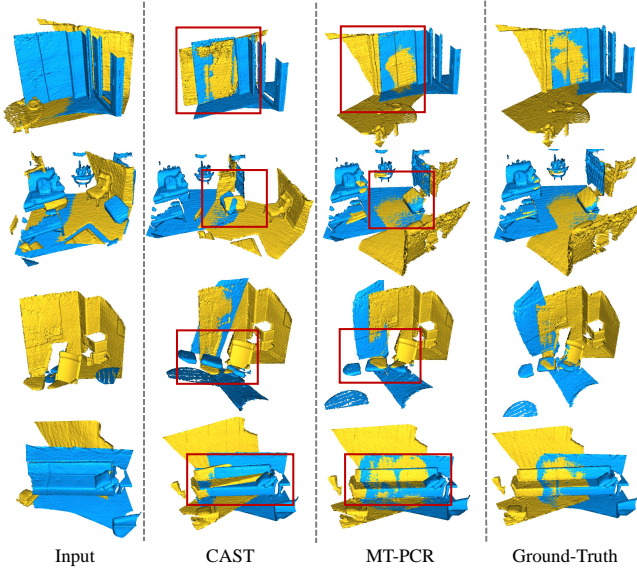


Figure 4: Qualitative registration results of CAST and MT-PCR compared with the ground truth alignment on 3DMatch dataset. We present four examples in four rows, which demonstrate the robustness and accuracy of our method.

Table 3: Efficiency Comparison at Varying Token Lengths. Computational efficiency for different methods across increasing token lengths.

Length of Token	128	256	512	768	1024	1536
	GFLOPs ↓					
GeoTrans [32]	16	62	244	547	969	out of memory
CAST [19]	6	18	63	129	218	430
MT-PCR (ours)	4	12	39	80	129	258
	GPU Memory (MB) ↓					
GeoTrans [32]	176	634	2463	5510	12335	out of memory
CAST [19]	120	334	1185	2491	4189	11028
MT-PCR (ours)	119	335	1162	2428	4091	10591
	FPS ↑					
GeoTrans [32]	5.97	5.43	4.79	3.27	2.83	out of memory
CAST [19]	6.52	6.19	5.27	4.50	3.69	2.63
MT-PCR (ours)	6.17	5.92	5.22	4.59	4.02	3.00

Effect of Point Cloud Serialization. We next examine the impact of different serialization strategies using spatial space-filling curves. In particular, we compare the performance of two representative curves: Hilbert and Z-order, along with their axis-permuted variants: Trans-Hilbert and Trans-Z-order. We also include the commonly used XYZ-order and its variant as baselines.

As shown in Table 4, methods using space-filling curve serialization outperform traditional baselines, with the Z-order strategy achieving the best overall performance. We attribute this to the locality-preserving nature of space-filling curves, which provide

Table 4: Ablation studies on serialization strategies.

Strategy	RR (%)	PMR (%)	PIR (%)
baseline	93.47	96.24	76.84
hilbert \times 3	94.36	96.42	77.09
hilbert ^T \times 3	94.08	95.97	75.10
hilbert, hilbert ^T , z	95.07	96.84	78.83
xyz, zxy, yxz	94.00	96.33	76.57
z ^T \times 3	94.37	96.51	78.16
z \times 3	95.54	96.87	79.65

Table 5: Ablation studies on linear attention methods.

Model	RR (%)	PMR (%)	PIR (%)
Based [3]	94.75	96.33	78.24
Samba [33]	94.44	96.06	76.46
Metala [9]	94.53	95.36	73.17
Transformer [37]	94.96	95.88	75.54
Mamba	95.54	96.87	79.65

Table 6: Ablation studies on order strategies.

Setting	RR (%)	PMR (%)	PIR (%)
None	95.54	96.87	79.65
Order indicator	94.74	96.42	77.75

more logically ordered sequences for state space models. This continuous spatial scanning offers a natural inductive bias for Mamba to model geometry-aware sequences.

Effectiveness of Mamba. In addition to Mamba, several newly proposed models with linear computational complexity have recently emerged, as shown in Table 5. To evaluate their effectiveness in the context of PCR, we conducted ablation studies comparing Mamba with representative linear attention models. The results suggest that the improved Mamba variant achieves the best performance among these linear models and even surpasses Transformer-based models in registration accuracy.

Effectiveness of Indicator. As shown in Table 6, we identify that the order indicator module, commonly adopted in Point Mamba [23], is unnecessary in our context, and its removal leads to improved performance in the PCR tasks.

6 Conclusion

In this paper, we introduced MT-PCR, the first hierarchical point cloud registration framework that unifies the strengths of both Mamba and Transformer architectures. By leveraging the linear complexity and long-range modeling capabilities of Mamba, along

with the spatially aware refinement of Transformers, our framework addresses the scalability limitations of existing Transformer-based PCR methods. To bridge the gap between sequence-based models and unordered 3D point clouds, we proposed a feature serialization approach based on Z-order space-filling curves, which preserves spatial locality and enhances the compatibility of point cloud features with Mamba. Additionally, we observed that removing the conventional order-indicator tokens—commonly used in sequential modeling—leads to superior registration performance, highlighting a useful design insight for applying state space models to geometric data. Comprehensive experiments on challenging benchmarks such as 3DMatch, 3DLoMatch, and KITTI demonstrate that MT-PCR not only achieves state-of-the-art accuracy but also significantly improves computational efficiency by reducing both GPU memory consumption and FLOPs. We believe that the hybrid design principles of MT-PCR open up new opportunities for efficient and scalable 3D perception and provide a promising direction for future research in point cloud representation learning and registration.

References

- [1] Sheng Ao, Qingyong Hu, Hanyun Wang, Kai Xu, and Yulan Guo. 2023. Buffer: Balancing accuracy, efficiency, and generalizability in point cloud registration. In *Proceedings of the IEEE/CVF Conference on Computer Vision and Pattern Recognition*. 1255–1264.
- [2] Sheng Ao, Qingyong Hu, Bo Yang, Andrew Markham, and Yulan Guo. 2021. Spinnet: Learning a general surface descriptor for 3d point cloud registration. In *Proceedings of the IEEE/CVF Conference on Computer Vision and Pattern Recognition*. 11753–11762.
- [3] Simran Arora, Sabri Eyuboglu, Michael Zhang, Aman Timalina, Silas Alberti, Dylan Zinsley, James Zou, Atri Rudra, and Christopher Ré. 2024. Simple linear attention language models balance the recall-throughput tradeoff. *ArXiv preprint abs/2402.18668* (2024). <https://arxiv.org/abs/2402.18668>
- [4] Xuyang Bai, Zixin Luo, Lei Zhou, Hongbo Fu, Long Quan, and Chiew-Lan Tai. 2020. D3feat: Joint learning of dense detection and description of 3d local features. In *Proceedings of the IEEE/CVF Conference on Computer Vision and Pattern Recognition*. 6359–6367.
- [5] Cesar Cadena, Luca Carlone, Henry Carrillo, Yasir Latif, Davide Scaramuzza, José Neira, Ian Reid, and John J Leonard. 2016. Past, present, and future of simultaneous localization and mapping: Toward the robust-perception age. *IEEE Transactions on robotics* 32, 6 (2016), 1309–1332.
- [6] Julie Carmigniani, Borko Furht, Marco Anisetti, Paolo Ceravolo, Ernesto Damiani, and Misa Ivkovic. 2011. Augmented reality technologies, systems and applications. *Multimedia tools and applications* 51 (2011), 341–377.
- [7] Suyi Chen, Hao Xu, Ru Li, Guanghui Liu, Chi-Wing Fu, and Shuaicheng Liu. 2023. SIRA-PCR: Sim-to-Real Adaptation for 3D Point Cloud Registration. In *Proceedings of the IEEE/CVF International Conference on Computer Vision*. 14394–14405.
- [8] Zhi Chen, Yufan Ren, Tong Zhang, Zheng Dang, Wenbing Tao, Sabine Süstrunk, and Mathieu Salzmann. 2023. Diffusionpcr: Diffusion models for robust multi-step point cloud registration. *arXiv preprint arXiv:2312.03053* (2023).
- [9] Yuhong Chou, Man Yao, Kexin Wang, Yuqi Pan, Rui-Jie Zhu, Jibin Wu, Yiran Zhong, Yu Qiao, Bo Xu, and Guoqi Li. 2024. MetaLA: Unified optimal linear approximation to softmax attention map. *Advances in Neural Information Processing Systems* 37 (2024), 71034–71067.
- [10] Christopher Choy, Jaesik Park, and Vladlen Koltun. 2019. Fully convolutional geometric features. In *Proceedings of the IEEE/CVF International Conference on Computer Vision*. 8958–8966.
- [11] Haowen Deng, Tolga Birdal, and Slobodan Ilic. 2018. Ppfnet: Global context aware local features for robust 3d point matching. In *Proceedings of the IEEE Conference on Computer Vision and Pattern Recognition*. 195–205.
- [12] MA FISCHLER AND. 1981. Random sample consensus: a paradigm for model fitting with applications to image analysis and automated cartography. *Commun. ACM* 24, 6 (1981), 381–395.
- [13] Andreas Geiger, Philip Lenz, and Raquel Urtasun. 2012. Are we ready for autonomous driving? the kitti vision benchmark suite. In *IEEE Conference on Computer Vision and Pattern Recognition*. IEEE, 3354–3361.
- [14] Zan Gojcic, Caifa Zhou, Jan D Wegner, and Andreas Wieser. 2019. The perfect match: 3d point cloud matching with smoothed densities. In *Proceedings of the IEEE/CVF Conference on Computer Vision and Pattern Recognition*. 5545–5554.
- [15] Albert Gu and Tri Dao. 2023. Mamba: Linear-Time Sequence Modeling with Selective State Spaces. *arXiv preprint arXiv:2312.00752* (2023).
- [16] Albert Gu, Karan Goel, Ankit Gupta, and Christopher Ré. 2022. On the parameterization and initialization of diagonal state space models. *Advances in Neural Information Processing Systems* 35 (2022), 35971–35983.
- [17] Shiyi Guo, Yihong Wu, Binjian Xie, Bingxi Liu, and Tong Jia. 2024. Low-Overlap Point Cloud Registration by Semiglobal Block Matching. *IEEE Transactions on Industrial Informatics* (2024).
- [18] Xu Han, Yuan Tang, Zhaoxuan Wang, and Xianzhi Li. 2024. Mamba3d: Enhancing local features for 3d point cloud analysis via state space model. In *Proceedings of the 32nd ACM International Conference on Multimedia*. 4995–5004.
- [19] Renlang Huang, Yufan Tang, Jiming Chen, and Liang Li. 2024. A consistency-aware spot-guided transformer for versatile and hierarchical point cloud registration. *Proc. Conf. Neural Inf. Process. Syst.* (2024).
- [20] Shengyu Huang, Zan Gojcic, Mikhail Usvyatsov, Andreas Wieser, and Konrad Schindler. 2021. Predator: Registration of 3d point clouds with low overlap. In *Proceedings of the IEEE/CVF Conference on Computer Vision and Pattern Recognition*. 4267–4276.
- [21] Rudolph Emil Kalman. 1960. A new approach to linear filtering and prediction problems. (1960).
- [22] Jiaxin Li and Gim Hee Lee. 2019. Usip: Unsupervised stable interest point detection from 3d point clouds. In *Proceedings of the IEEE/CVF International Conference on Computer Vision*. 361–370.
- [23] Dingkan Liang, Xin Zhou, Wei Xu, Xingkui Zhu, Zhikang Zou, Xiaoqing Ye, Xiao Tan, and Xiang Bai. 2024. PointMamba: A Simple State Space Model for Point Cloud Analysis. In *Advances in Neural Information Processing Systems*.
- [24] Jiuming Liu, Ruiji Yu, Yian Wang, Yu Zheng, Tianchen Deng, Weicai Ye, and Hesheng Wang. 2024. Point mamba: A novel point cloud backbone based on state space model with octree-based ordering strategy. *arXiv preprint arXiv:2403.06467* (2024).
- [25] Yue Liu, Yunjie Tian, Yuzhong Zhao, Hongtian Yu, Lingxi Xie, Yaowei Wang, Qixiang Ye, Jianbin Jiao, and Yunfan Liu. 2024. Vmamba: Visual state space model. *Advances in neural information processing systems* 37 (2024), 103031–103063.
- [26] Ilya Loshchilov and Frank Hutter. 2018. Decoupled Weight Decay Regularization. In *International Conference on Learning Representations*.
- [27] Fan Lu, Guang Chen, Yinlong Liu, Lijun Zhang, Sanqing Qu, Shu Liu, Rongqi Gu, and Changjun Jiang. 2023. HRegNet: A hierarchical network for efficient and accurate outdoor LiDAR point cloud registration. *IEEE Transactions on Pattern Analysis and Machine Intelligence* (2023).
- [28] Weixin Lu, Yao Zhou, Guowei Wan, Shenhua Hou, and Shiyu Song. 2019. L3-net: Towards learning based lidar localization for autonomous driving. In *Proceedings of the IEEE/CVF conference on computer vision and pattern recognition*. 6389–6398.
- [29] Aaron van den Oord, Yazhe Li, and Oriol Vinyals. 2018. Representation learning with contrastive predictive coding. *arXiv preprint arXiv:1807.03748* (2018).
- [30] Adam Paszke, Sam Gross, Francisco Massa, Adam Lerer, James Bradbury, Gregory Chanan, Trevor Killeen, Zeming Lin, Natalia Gimelshein, Luca Antiga, Alban Desmaison, Andreas Kopf, Edward Yang, Zachary DeVito, Martin Raison, Alykhan Tejani, Sasank Chilamkurthy, Benoit Steiner, Lu Fang, Junjie Bai, and Soumith Chintala. 2019. PyTorch: An Imperative Style, High-Performance Deep Learning Library. In *Advances in Neural Information Processing Systems*, Vol. 32.
- [31] Charles R Qi, Hao Su, Kaichun Mo, and Leonidas J Guibas. 2017. Pointnet: Deep learning on point sets for 3d classification and segmentation. In *Proceedings of the IEEE Conference on Computer Vision and Pattern Recognition*. 652–660.
- [32] Zheng Qin, Hao Yu, Changjian Wang, Yulan Guo, Yuxing Peng, Slobodan Ilic, Dewen Hu, and Kai Xu. 2023. GeoTransformer: Fast and Robust Point Cloud Registration With Geometric Transformer. *IEEE Transactions on Pattern Analysis and Machine Intelligence* (2023).
- [33] Liliang Ren, Yang Liu, Yadong Lu, Yelong Shen, Chen Liang, and Weizhu Chen. 2024. Samba: Simple Hybrid State Space Models for Efficient Unlimited Context Language Modeling. *ArXiv preprint abs/2406.07522* (2024). <https://arxiv.org/abs/2406.07522>
- [34] Radu Bogdan Rusu, Nico Blodow, and Michael Beetz. 2009. Fast point feature histograms (FPFH) for 3D registration. In *2009 IEEE International Conference on Robotics and Automation*. IEEE, 3212–3217.
- [35] Radu Bogdan Rusu, Nico Blodow, Zoltan Csaba Marton, and Michael Beetz. 2008. Aligning point cloud views using persistent feature histograms. In *2008 IEEE/RSJ International Conference on Intelligent Robots and Systems*. IEEE, 3384–3391.
- [36] Samuele Salti, Federico Tombari, and Luigi Di Stefano. 2014. SHOT: Unique signatures of histograms for surface and texture description. *Computer Vision and Image Understanding* 125 (2014), 251–264.
- [37] Ashish Vaswani, Noam Shazeer, Niki Parmar, Jakob Uszkoreit, Llion Jones, Aidan N Gomez, Łukasz Kaiser, and Illia Polosukhin. 2017. Attention is all you need. *Advances in neural information processing systems* 30 (2017).
- [38] Haiping Wang, Yuan Liu, Zhen Dong, and Wenping Wang. 2022. You only hypothesize once: Point cloud registration with rotation-equivariant descriptors. In *Proceedings of the 30th ACM International Conference on Multimedia*. 1630–1641.
- [39] Jingtao Wang and Zechao Li. 2024. 3DPCP-Net: A Lightweight Progressive 3D Correspondence Pruning Network for Accurate and Efficient Point Cloud Registration. In *Proceedings of the 32nd ACM International Conference on Multimedia*.

- 1885–1894.
- [40] Yue Wang and Justin M Solomon. 2019. Deep closest point: Learning representations for point cloud registration. In *Proceedings of the IEEE/CVF international conference on computer vision*. 3523–3532.
 - [41] Fan Yang, Lin Guo, Zhi Chen, and Wenbing Tao. 2022. One-inlier is first: Towards efficient position encoding for point cloud registration. *Advances in Neural Information Processing Systems* 35 (2022), 6982–6995.
 - [42] Heng Yang, Jingnan Shi, and Luca Carlone. 2020. Teaser: Fast and certifiable point cloud registration. *IEEE Transactions on Robotics* 37, 2 (2020), 314–333.
 - [43] Zi Jian Yew and Gim Hee Lee. 2018. 3dfeat-net: Weakly supervised local 3d features for point cloud registration. In *Proceedings of the European Conference on Computer Vision (ECCV)*. 607–623.
 - [44] Zi Jian Yew and Gim Hee Lee. 2022. Regtr: End-to-end point cloud correspondences with transformers. In *Proceedings of the IEEE/CVF Conference on Computer Vision and Pattern Recognition*. 6677–6686.
 - [45] Hao Yu, Fu Li, Mahdi Saleh, Benjamin Busam, and Slobodan Ilic. 2021. Cofinet: Reliable coarse-to-fine correspondences for robust point cloud registration. *Advances in Neural Information Processing Systems* 34 (2021), 23872–23884.
 - [46] Hao Yu, Zheng Qin, Ji Hou, Mahdi Saleh, Dongsheng Li, Benjamin Busam, and Slobodan Ilic. 2023. Rotation-invariant transformer for point cloud matching. In *Proceedings of the IEEE/CVF Conference on Computer Vision and Pattern Recognition*. 5384–5393.
 - [47] Junle Yu, Luwei Ren, Yu Zhang, Wenhui Zhou, Lili Lin, and Guojun Dai. 2023. PEAL: Prior-embedded explicit attention learning for low-overlap point cloud registration. In *Proceedings of the IEEE/CVF Conference on Computer Vision and Pattern Recognition*. 17702–17711.
 - [48] Andy Zeng, Shuran Song, Matthias Nießner, Matthew Fisher, Jianxiong Xiao, and Thomas Funkhouser. 2017. 3dmatch: Learning local geometric descriptors from rgb-d reconstructions. In *Proceedings of the IEEE Conference on Computer Vision and Pattern Recognition*. 1802–1811.
 - [49] Xiyu Zhang, Jiaqi Yang, Shikun Zhang, and Yanning Zhang. 2023. 3D registration with maximal cliques. In *Proceedings of the IEEE/CVF Conference on Computer Vision and Pattern Recognition*. 17745–17754.
 - [50] Lianghui Zhu, Bencheng Liao, Qian Zhang, Xinlong Wang, Wenyu Liu, and Xinggang Wang. [n. d.]. Vision Mamba: Efficient Visual Representation Learning with Bidirectional State Space Model. In *Forty-first International Conference on Machine Learning*.